Appl Magn Reson (2010) 37:27–37
DOI 10.1007/s00723-009-0037-z

Applied
Magnetic Resonance

Electronic Structure of Fe^{3+} at a Metal-Binding Site Introduced in Modified Bacterial Reaction Centers

L. Kálmán · M. Flores · J. C. Williams · J. P. Allen

Received: 27 May 2009 / Revised: 26 June 2009 / Published online: 13 November 2009

Abstract The electronic structure of Fe^{3+} was studied in a mutant that has been modified to bind manganese or iron at a site corresponding to the manganese-binding site of photosystem II (Kálmán et al., Biochemistry 45:13869–13874, 2006). Using electron paramagnetic resonance spectroscopy, the presence of the oxidized state of the bacteriochlorophyll dimer, $P^{\cdot+}$, was detected in the light when no metal was added. When iron was bound to the modified reaction centers in the presence of bicarbonate, the contribution of $P^{\cdot+}$ was greatly reduced and a signal characteristic of Fe^{3+} was evident. To characterize the electronic structure of this ferric ion, the electron paramagnetic resonance spectrum was measured at X-band at temperatures from 4 to 200 K. The major contribution to the spectrum at 4 K is from Fe^{3+} with a spin 3/2 in a rhombic coordination and E/D ratio of 0.1914 and g_{eff} values of 6.0, 2.9, and 2.0. As the temperature increases from 4 to 200 K, the signal shifts, with the central g_{eff} value changing from 2.9 to 2.2. This change with temperature may result from alterations in the interaction with the bicarbonate coordinated to the iron as the temperature increases.

1 Introduction

In photosynthetic bacteria, light energy is converted into chemical energy through a chain of electron transfer processes, with the primary photochemistry occurring in an integral membrane protein termed the reaction center [1, 2]. The absorption of

L. Kálmán · M. Flores · J. C. Williams · J. P. Allen (✉)
Department of Chemistry and Biochemistry, Arizona State University,
Tempe, AZ 85287-1604, USA
e-mail: JAllen@asu.edu

Present Address:
L. Kálmán
Department of Physics, Concordia University, Montreal, QC, Canada

light results in the excitation of the primary electron donor, P, which is a bacteriochlorophyll dimer, followed by electron transfer from P to a series of acceptors, including the primary and secondary quinone acceptors, Q_A and Q_B, respectively. The oxidized bacteriochlorophyll dimer, $P^{\cdot+}$, is subsequently reduced by a water-soluble cytochrome c_2 allowing another photon of light to be absorbed. After the second electron transfer, Q_B leaves the reaction center and is replaced with a quinone from the quinone pool. In cyanobacteria, algae, and plants, excitation of the primary electron donor, P680, of photosystem II also results in a series of electron transfer steps from the primary donor to a quinone [3]. However, the primary donor is highly oxidizing, and the reduction of $P680^{\cdot+}$ involves a proton–electron coupled reaction with a tyrosine residue, Y_Z, followed by electron transfer from the manganese cluster. After absorption of four photons, water is oxidized at the manganese cluster forming molecular oxygen.

Despite these differences in their functions, the three-dimensional (3D) structures show that the core structures of the reaction center and photosystem II are homologous [4–7]. This structural homology provides an opportunity to mimic some of the properties of photosystem II associated with water oxidation in the reaction center from *Rhodobacter sphaeroides* [8]. The primary donor in wild-type reaction centers does not have a sufficient oxidation/reduction midpoint potential to oxidize tyrosine or manganese. Therefore, a series of mutations were designed that made the primary donor of the reaction center highly oxidizing, resulting in the $P/P^{\cdot+}$ midpoint potential being increased to over 0.8 V [9]. These highly oxidizing reaction centers were able to oxidize tyrosine residues that were introduced at different sites [10, 11].

Mutations were introduced into these highly oxidizing reaction centers to provide manganese-binding ligands at a location comparable to the binding site of the manganese cluster of photosystem II [12, 13]. Four combinations of different possible manganese ligands were introduced in mutants. One of these, the M2 mutant, tightly binds manganese with a dissociation constant of 1 μM, while two others, the M1 and M4 mutants, bound manganese less tightly. The binding of manganese to the M3 mutant was similar to the binding in the control mutant that lacks the added ligands and binds manganese weakly and non-specifically. Spectroscopic studies showed that the manganese was capable of serving as a secondary electron donor to the oxidized bacteriochlorophyll dimer, $P^{\cdot+}$. The structure of reaction centers with manganese bound at the designed site was determined for the M2 mutant (Fig. 1). The metal interacts with three carboxylates, a histidine, and a bound water molecule, including the two groups introduced by mutagenesis, Glu at M168 and Asp at M288. Although no structure has been determined for the M1 mutant, its similarity to the M2 mutant suggests a related 3D structure, except for two differences: Glu in place of Val M192, and Gly in place of Asp M288.

The metal-binding sites of several proteins are capable of coordinating either manganese or iron cofactors. For example, the iron cofactor of ribonucleotide reductase can be replaced with manganese, and manganese has been observed at the iron-binding site of hemerythrin [14, 15]. This versatility of metal-binding sites in proteins led us to investigate the ability of the modified reaction centers to bind iron [16]. In the M1 and M2 mutants, $P^{\cdot+}$ was reduced by the bound ferrous ion with

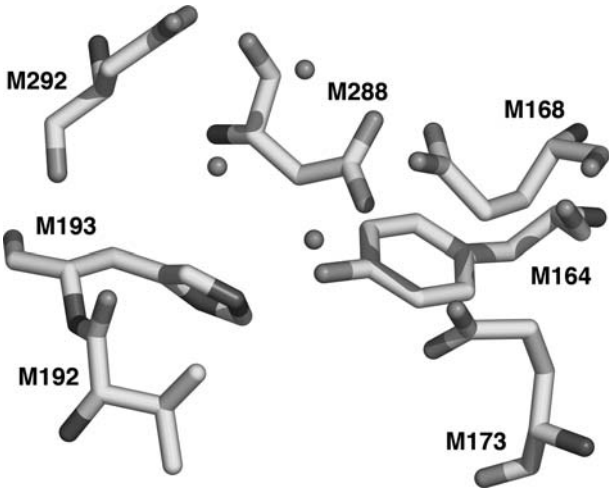

Fig. 1 3D structure of the reaction center from the M2 mutant of *R. sphaeroides* determined using X-ray diffraction [12] showing the presence of a bound Mn atom (*sphere* in center of figure) and the nearby amino acid residues (shaded according to atom type): Tyr M164, Glu M168, Glu M173, Val M192, His M193, Asp M288, and Glu M292. Also shown are two bound water molecules (*small spheres*). For the M2 mutant, the introduced changes at the binding site were Arg M164 to Tyr, Met 168 to Glu and Gly M288 to Asp. The M1 mutant has two differences compared to the M2 mutant: M192 is Glu rather than Val and M288 remains Gly as found for wild type. The changes of Arg M164 to Tyr and Met M168 to Glu compared to wild type are found in both mutants. Coordinates of the M2 structure are from the Protein Data Bank, file 1Z9J [12]

first-order rates in the presence of sodium bicarbonate with dissociation constants of ~ 1 μM.

The techniques of electron paramagnetic resonance (EPR) and electron-nuclear double resonance (ENDOR) spectroscopy are ideally suited for the characterization of charge-separated states. Indeed, EPR was one of the initial techniques used to characterize the oxidation states of the bacterial reaction center and provided the experimental data used in the identification of the primary electron donor as a bacteriochlorophyll dimer [17]. Since those initial studies, both EPR and ENDOR studies have been performed on the charge-separated state $P^{\cdot+}Q_A^{\cdot-}$, leading to a molecular understanding of the electronic structure of $P^{\cdot+}$ and $Q_A^{\cdot-}$ [18–20]. In the case of the modified mutants with bound iron, the charge-separated state is $Fe^{3+}PQ_A^{\cdot-}$, which provides the opportunity to probe the character of the bound Fe^{3+} [16]. In this study, the electronic structure of the iron bound to the M1 mutant is probed by measurement of the temperature dependence of the EPR spectrum of the oxidized iron.

2 Methods

2.1 Construction of the Mutants and Protein Isolation

The M1 mutant was constructed in *R. sphaeroides* as described elsewhere [12]. The M1 mutant incorporates the changes L131 Leu to His, M160 Leu to His and M197

Phe to His, each of which increases the $P/P^{\cdot+}$ potential by altering the hydrogen-bonding pattern of the dimer [21]. In addition to these three mutations, the M1 mutant contains three further changes. M164 Arg has been replaced with a neutral Tyr, and two carboxylic residues were introduced to serve as ligands to the metal using the following mutations: M168 Met to Glu and M192 Val to Glu.

2.2 Sample Preparation

Cells were grown semiaerobically and reaction centers were isolated and purified as described earlier, except that the detergent lauryidimethylamine oxide (LDAO) has been replaced with Triton X-100 in the ion exchange chromatography step [22]. Any ethylenediaminetetraacetic acid (EDTA) was removed by extensive ($\sim$48 h) dialysis against 0.03% Triton X-100, 15 mM 4-(2-hydroxyethyl)-1-piperazineethanesulfonic acid (HEPES), pH 7. Measurements were performed in the presence of excess terbutryne to block electron transfer to the secondary quinone, Q_B. The solutions were prepared and stored under nitrogen atmosphere, and the ferrous iron sulfate solutions were prepared immediately prior to use to avoid autooxidation of the iron (II) caused by dissolved oxygen. In the measurements of metal binding, bicarbonate was included such that the final concentration was poised at 15 mM to facilitate the metal binding [23]. A ferrous-sulfate solution was added to diluted (1 μM) reaction centers in threefold excess concentration. After 15–20 min incubation, the reaction centers with bound iron were concentrated using Centricon microconcentrators (Millipore, Billerica MA, USA) up to a protein concentration of approximately 50 μM. Since any unbound metal passes through the filter, the presence of free iron in the samples is minimized. Prior to the measurement, sodium bicarbonate and terbutyrne were added at final concentrations of 20 mM and 300 μM, respectively, followed by addition of glycerol, poised at a final concentration of 50%, as a cryoprotectant agent.

2.3 EPR Spectroscopy

Spectra were recorded using a Bruker E580 X-band spectrometer (Bruker, Silberstreifen, Germany) equipped with an Oxford Model 900 EPL liquid helium cryostat (Oxford Instruments, Oxfordshire, UK). The magnetic field modulation frequency was 100 kHz, the amplitude was 0.4 mT, the microwave power was 10 mW, and the microwave frequency was approximately 9.41 GHz. The sweep time was 335.54 s. The light-induced radicals were "freeze-trapped" by immersing the samples into liquid nitrogen during illumination.

2.4 Fitting of EPR Spectra

The EPR spectra were simulated using EasySpin (v 3.0.0), a computational package developed by Stoll and Schweiger [24] and based on Matlab (The MathWorks, Natick, MA, USA). Both the 3/2 and 5/2 spins of Fe^{3+} were considered in the simulations using a fitting procedure similar to that described by Flores et al. [18]. The fitting parameters were the following: the three g values, g_x, g_y, and g_z, the line width, ΔB, and the zero-field splitting parameters, D and E.

3 Results

In our initial experiments, EPR spectra were measured at 120 K under different experimental conditions for reaction centers isolated from the M1 mutant (Fig. 2). In the dark, no prominent signals are evident; the lack of any signals is consistent with the absence of any charge-separated states in the dark. In the light but without added iron, a narrow signal centered at a g_{eff} value of 2.0 is seen in the EPR spectrum. This signal is assigned to the species $P^{\cdot+}$. The $Q_A^{\cdot-}$ species is also generated under these conditions but is not observed at this temperature due to a broadening of the signal resulting from a coupling with the non-heme Fe^{2+} located near the quinones in the native reaction center. In the presence of both light and added iron, strong signals are present at g_{eff} values of 4.3 and 2.2 with a significant reduction in the relative contribution of the $P^{\cdot+}$ signal. The reduction of the $P^{\cdot+}$ signal and the presence of the new signals are consistent with the rapid reduction of $P^{\cdot+}$ by the iron, resulting in the conversion of the iron from Fe^{2+} to Fe^{3+} as reported previously [16]. In all cases, a small signal at a g_{eff} value of 4.3 representing a minor contribution of Fe^{3+} is present in the samples of the reaction center mutants due to oxidation of bound iron during the sample preparation.

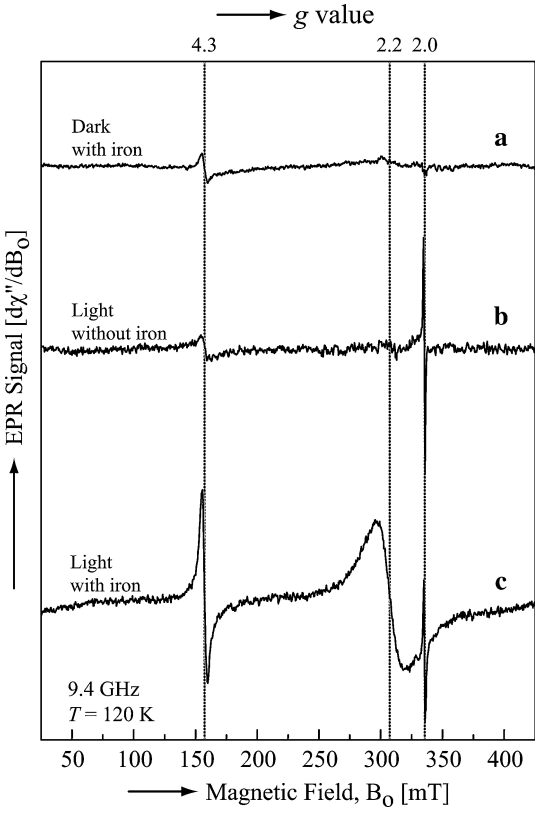

Fig. 2 EPR spectra of reaction centers from the M1 mutant under different conditions measured at 120 K. *a* In the dark with added iron present no strong signals are evident. *b* In the light without added iron a signal is seen near a *g* value of 2.0 due to the presence of $P^{\cdot+}$. *c* In the light with added iron, signals centered at g_{eff} values of 4.3 and 2.2 are seen due to the presence of bound Fe^{3+} with a significant reduction in the contribution of the signal at a *g* value of 2.0 due to $P^{\cdot+}$. All three spectra contain a small contribution from Fe^{3+} because of oxidation of the iron that is present in the sample preparations. The traces shown are from single scans measured at 120 K and a frequency of 9.4 GHz

To understand the nature of the light-induced states observed in these spectra, EPR measurements were recorded for the M1 mutant at temperatures ranging from 200 to 4 K (Fig. 3). As the temperature was decreased, a number of spectral changes were observed. The signal at a g value of 4.3 increased in amplitude as the temperature was decreased. A signal at a g value of 2.3 detected at 200 K appears to shift to a g value of 2.2 as the temperature decreases to 120 K. Further cooling resulted in the presence of a signal centered near a g value of 2.9 and the reduction of the signal at a g value of 2.2. Since these signals are all evident only in the presence of both light and iron, they are assigned as arising from the presence of Fe^{3+} bound at the designed site.

In addition to the signals from the bound iron, two other contributions are evident. The signal from $P^{\cdot+}$ was observed at every temperature at a g_{eff} value of 2.0 because of the presence of a small fraction of the reaction centers without a bound iron. At 10 K and below, a signal near a g_{eff} value of 1.8 is observed; this signal is due to the semiquinone signal that is broadened as a result of its magnetic coupling to the central ferrous iron ($Q_A^{\cdot-}Fe^{2+}$) [25]. Unlike the iron bound at the designed site, the central nonheme iron remains in the Fe^{2+} state throughout the electron transfer processes and is observed only through its coupling to the semiquinone. These two contributions are present in all reaction centers and are unchanged in the mutant

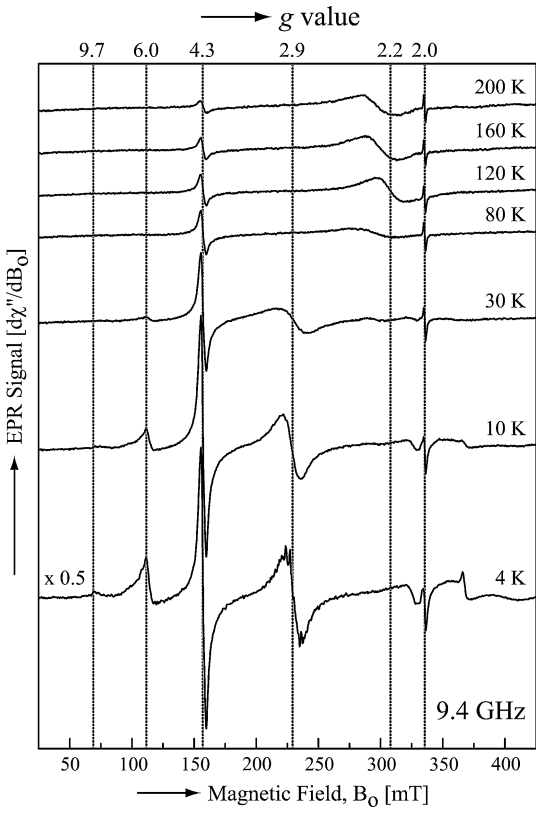

Fig. 3 EPR spectra of reaction centers from the M1 mutant in the present of light and added iron at temperatures ranging from 200 to 4 K. The traces shown are from single scans measured at temperatures ranging from 4 to 200 K and a frequency of 9.4 GHz

compared to wild type, demonstrating that the mutant was largely unchanged except for the presence of iron at the designed metal-binding site.

4 Discussion

In wild-type reaction centers, light absorption results in the formation of the charge-separated state $P^{\cdot+}Q_A^{\cdot-}$ when terbutryne is present to block electron transfer between the quinones. For the mutant reaction centers, a metal-binding site has been introduced at a location approximately 10 Å from P. When manganese or iron is bound at this site, the metal can rapidly reduce $P^{\cdot+}$ as shown by optical studies of the mutant that confirm the loss of the $P^{\cdot+}$ signal [12, 13, 16]. These studies also use EPR to demonstrate that when iron is bound at this site, the species Fe^{3+} is formed. In this work, we characterized the electronic structure of the Fe^{3+} by an analysis of the light-induced EPR signals at temperatures ranging from 4 to 200 K.

The EPR spectra have revealed a number of structural characteristics of the metal-binding mutant. The EPR signals are present only after illumination and with the addition of iron, as the dark spectrum is featureless and the iron-free samples show only a contribution from $P^{\cdot+}$ (Fig. 2). Thus, the new signals are assigned as arising from the presence of Fe^{3+} bound at the designed site. The spectra showed a number of new features that can be divided into two sets based upon their temperature dependence (Fig. 3). One set of spectral features shows a pronounced temperature dependence. This set has signals at g_{eff} values of 6.0 and 2.0 that are only evident at temperatures below 30 K and a signal centered at a g_{eff} value of 2.9 below 30 K and values of 2.3 to 2.2 above 80 K. The second set of features at g_{eff} values of 9.7 and 4.3 are independent of temperature except for the amplitude change expected based upon a Boltzmann temperature dependence. Comparison of the integrated intensity of these two sets of features shows that the temperature-dependent set is dominant, with a contribution more than 80% compared to the temperature-independent features.

4.1 Detailed Analysis of EPR Spectra

The signals that show a significant dependence of the g values on temperature have g_{eff} values of 6.0, 2.9, and 2.0 in the spectrum at 4 K. These spectral features are well fitted by assuming the presence of an intermediate spin of 3/2 and E/D ratio of approximately 0.191 (Fig. 4). They correspond to resonances within the $m_s = \pm 1/2$ Kramers doublet of a spin system 3/2 with large zero-field splitting ($D >> g\beta B_o$) and moderately strong rhombicity E/D (Table 1). Since the spectrum is detected at liquid helium temperature, $m_s = \pm 1/2$ must be the ground doublet, consistent with a positive D value. Thus, the Fe^{3+} binds at the designed site with a rhombic coordination. These signals are present in the spectra at temperatures below 80 K but are not evident at temperatures of 120 K and above. The simplest explanation is that the new signals at g_{eff} values of 2.3 to 2.2 arise from the same species but the coordination of the Fe^{3+} changes at the higher temperatures causing a change in the g_{eff} values. This hypothesis is supported by the fact that resonances within the $m_s = \pm 3/2$ Kramers doublet, corresponding to the low temperature species ($S = 3/2$),

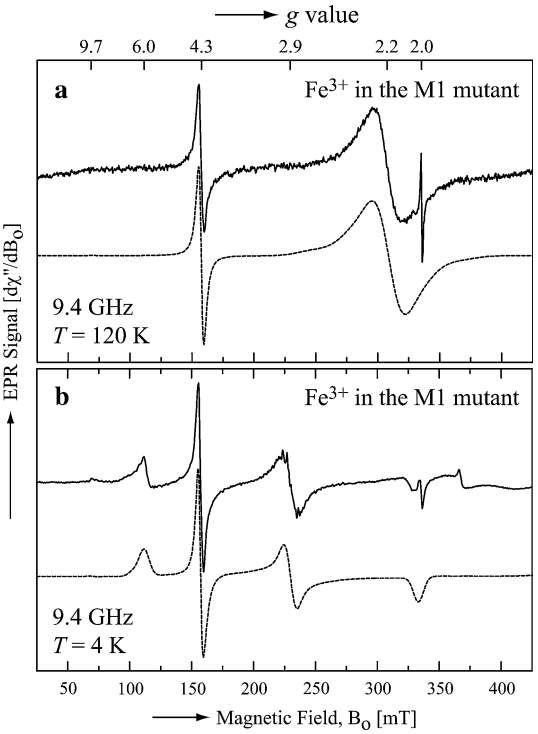

Fig. 4 Experimental (*solid lines*) and simulated (*dotted lines*) EPR spectra of Fe^{3+} bound to reaction centers from the M1 mutant at temperatures of **a** 120 K and **b** 4 K. The EPR spectra were fitted by considering the possibility of a 5/2 or 3/2 spin state of the Fe^{3+}. In both cases, the spectra have contributions of P^{+} and Q_A^{-} near *g* values of 2 and 1.8 that were not included in the simulations. The fitting parameters are summarized in Table 1. The two experimental spectra are the same as those shown in Fig. 3

are expected at higher magnetic fields (around $g_{eff} = 1.2$ when $D = 10^5$ MHz). At the higher temperatures, the signals are well described assuming that the iron is either in a 3/2 or 5/2 spin state. In both cases the *D* and *E* values are very small, less than the Zeeman splitting, resulting in an apparent isotropic signal.

At all the temperatures, there is a minor contribution at *g* values of 9.7 and 4.3. Part of this signal is due to a contribution from Fe^{3+} that is always present in the mutant samples because of minor oxidation during sample preparation. However, in the presence of light and added iron, most of the signal arises from a light-induced contribution. These signals are well fitted assuming a high-spin 5/2 state that also has rhombic symmetry with an *E*/*D* ratio of approximately 1/3, which represents the axial limit (Fig. 4; Table 1). Presumably, this contribution at a g_{eff} value of 9.7 and 4.3 also is due to iron bound at the designed site but with different interactions with the surrounding protein and bicarbonate.

4.2 Comparison with Other Metalloproteins and Model Compounds

The presence of both high- and intermediate-spin states for the bound iron is consistent with the properties of mononuclear iron ions in other proteins. For example, iron superoxide dismutase contains a mononuclear iron that is coordinated to three histidines, a carboxylate, and a bound water molecule and exhibits many of the same spectral features [26]. The spectrum of the wild-type superoxide dismutase has a derivative signal at a g_{eff} value of 4.3 that has been interpreted as arising from

Table 1 Parameters used in the fittings of EPR spectra of Fe^{3+} at the metal-binding site introduced in modified reaction centers (M1 mutant)

Parameters[a]	$T = 4$ K		$T = 120$ K	
	Species 1[b] ($S = 3/2$)	Species 2[c] ($S = 5/2$)	Species 1[b] ($S = 5/2$)	Species 2[c] ($S = 5/2$)
g_x	2.24	2.00	2.18	2.00
g_y	2.41	1.99	2.18	1.99
g_z	2.08	1.98	2.18	1.98
ΔB (mT)	9.7	7.3	26.1	7.0
D (MHz)[d]	$>10^{+5}$	$>10^{+5}$	$<5 \times 10^{+2}$	$>10^{+5}$
E/D	0.1914	1/3	0–0.333[d]	1/3

Two paramagnetic species were observed. The spectrum of each species was calculated independently (see Sect. 2)

[a] The fitting parameters were the following: the three g values, g_x, g_y, and g_z, the line width, ΔB, and the zero-field splitting parameters, D and E

[b] The electronic structure of this species is temperature-dependent. g values and zero-field parameters change with temperature

[c] The electronic structure of this species does not change with temperature. This species can also be described as a $S = 3/2$ state at T = 120 K

[d] These parameters could not be determined uniquely, only limits could be established

a high-spin Fe^{3+} [27]. Introduction of anions was found to alter the spectrum in a manner indicating a mixed binding configuration. For example, the iron can react with nitric oxide to yield a Fe–NO adduct that exhibits a spectrum at 4 K with two rhombic intermediate-spin signals of comparable population. The simulation of these spectra yielded large rhombicities, with E/D values of 0.128 and 0.154, and two sets of g_{eff} values near 4.8, 3.15, and 1.9. At the higher temperature of 30 K, the spectrum has an additional resonance at a g_{eff} value of 5.87 indicating a new contribution from a 3/2 spin. The influence of the anion is further shown by the result that the azide adduct of superoxide dismutase shows a spectrum with features at g_{eff} values of 9.8 and 4.3 that is modeled as arising from a high-spin iron with nearly rhombic symmetry [28]. These spectral features are very similar to what is observed for the modified reaction centers with bound iron. In particular, the observation of two spin states for the iron bound at the designed site in the reaction center and superoxide dismutase suggests that metals with associated anions may in general have multiple electronic states due to interactions involving residues or anions that directly coordinate or are near the metal at the binding site as discussed previously for superoxide dismutase [29].

The temperature dependence of the EPR spectra has similarities to that reported earlier for neuromelanin, a natural iron-binding protein [30, 31]. In that case, from temperatures of 300 to 120 K a broad absorption near a g_{eff} value of 2.1 is evident in the spectra. From 120 to 4 K this contribution is greatly diminished, and the spectra show signals near g_{eff} values of 4.3 and 2.6. In addition, another derivative signal is observed near a g value of 2.0 below 20 K. The spectra were interpreted as arising from two distinct species, one associated with the signals near g_{eff} values of 4.3 and the other for the signals near the 2.1 to 2.2 region of the spectrum. This strong

temperature dependence suggests that the involvement of ligands that do not arise from the protein may result in a metal coordination that changes at low temperatures.

The observation of an intermediate spin 3/2 state is unusual and unexpected for mononuclear Fe^{3+} bound as a cofactor in a protein. In inorganic model compounds, intermediate spin 3/2 states have been reported [32] and are typically related to a central ferric ion (Fe^{3+}) bound in a square planar configuration with strong ligands. In the reaction center, this type of coordination at the designed site is asymmetric and distorted due to the presence of different amino acid side chains serving as ligands (Fig. 1). However, the presence of the bicarbonate contributing to the coordination may favor a planar configuration due to the greater flexibility for the placement of the bicarbonate compared to the surrounding protein.

In summary, the EPR measurements are consistent with the conclusion that the addition of iron to the modified reaction centers leads to binding of the iron at the designed metal-binding site. After illumination, $P^{\cdot+}$ is rapidly reduced by the bound iron resulting in formation of a Fe^{3+} state. The temperature dependence of the EPR spectrum reveals two aspects of the electronic state of the Fe^{3+}. The iron is predominately in an intermediate-spin state with a rhombic configuration at 4 K with a minor high-spin state species also present. As the temperature increases to 200 K, the spectra change indicating a decrease in the magnitude of the crystal field interactions around the ferric iron (Fe^{3+}), i.e. from a regimen where $D >> g\beta B_o$ at 4 K to a regimen where $D << g\beta B_o$ at 200 K. Comparison with mononuclear iron cofactors in other proteins suggests that the observed spectral changes arise from changes in the interactions between the iron and the bound bicarbonate.

Acknowledgments This work was supported by a grant from the NSF (MCB 0640002). We thank Russ LoBrutto for assistance with the EPR measurements.

References

1. D.R. Ort, C.F. Yocum, *Oxygenic photosynthesis: the light reactions* (Kluwer, Dordrecht, 1996)
2. N. Hunter, F. Daldal, M. Thurnauer, J.T. Beatty, *The purple phototrophic bacteria* (Springer, Dordrecht, 2009)
3. T. Wydrzynski, K. Satoh, *Photosystem II: the light-driven water:plastoquinone oxidoreductase* (Springer, Dordrecht, 2005)
4. A. Zouni, H. T. Witt, J. Kern, P. Fromme, N. Krauss, W. Saenger, P. Orth, Nature **409**, 739–743 (2001)
5. N. Kamiya, J.R. Shen, Proc. Natl. Acad. Sci. USA **100**, 98–103 (2003)
6. K.N. Ferreira, T.M. Iverson, K. Maghlaoui, J. Barber, S. Iwata, Science **303**, 1831–1838 (2004)
7. A. Guskov, J. Kern, A. Gabdulkhakov, M. Broser, A. Zouni, W. Saenger, Nature Struct Molec. Biol. **16**, 334–342 (2009)
8. L. Kálmán, J.C. Williams, J.P. Allen, in *Photosystem II: The light-driven water:plastoquinone oxidoreductase*, ed. by T. Wydrzynski, K. Satoh (Springer, Dordrecht The Netherlands, 2005), pp. 715–727
9. L. Kálmán, R. LoBrutto, J.P. Allen, J.C. Williams, Nature **402**, 696–699 (1999)
10. L. Kálmán, A.J. Narváez, R. LoBrutto, J.C. Williams, J.P. Allen, Biochemistry **43**, 12905–12912 (2004)
11. A.J. Narváez, R. LoBrutto, J.P. Allen, J.C. Williams, Biochemistry **43**, 14379–14384 (2004)
12. M. Thielges, G. Uyeda, A. Cámara-Artigas, L. Kálmán, J.C. Williams, J.P. Allen, Biochemistry **44**, 7389–7394 (2005)

13. L. Kálmán, M.C. Thielges, J.C. Williams, J.P. Allen, Biochemistry **44**, 13266–13273 (2005)
14. M. Atta, P. Nordlund, A. Åberg, H. Eklund, M. Fontecave, J Biol. Chem. **267**, 20682–20688 (1992)
15. J.H. Zhang, D.M. Kurtz, Proc. Natl. Acad. Sci USA **89**, 7065–7069 (1992)
16. L. Kálmán, R. LoBrutto, J.C. Williams, J.P. Allen, Biochemistry **45**, 13869–13874 (2006)
17. G. Feher, J.P. Allen, M.Y. Okamura, D.C. Rees, Nature **339**, 111–116 (1989)
18. M. Flores, R. Isaacson, E. Abresch, R. Calvo, W. Lubitz, G. Feher, Biophys. J. **92**, 671–682 (2007)
19. G. Kothe, M.C. Thurnauer, Photosynth Res., in press (2009)
20. L. Kulik, W. Lubitz, Photosynth Res, in press (2009)
21. X. Lin, H.A. Murchison, V. Nagarajan, W.W. Parson, J.P. Allen, J.C. Williams, Proc Natl. Acad. Sci. USA **91**, 10265–10269 (1994)
22. J.C. Williams, R.G. Alden, H.A. Murchison, J.M. Peloquin, N.W. Woodbury, J.P. Allen, Biochemistry **31**, 11029–11037 (1992)
23. K. Tang, J.C. Williams, J.P. Allen, L. Kálmán, Biophys. J. **96**, 3295–3304 (2009)
24. S. Stoll, A. Schweiger, J. Magn. Reson. **178**, 42–55 (2006)
25. W.F. Butler, R. Calvo, D.R. Fredkin, R.A. Isaacson, M.Y. Okamura, G. Feher, Biophys. J. **45**, 947–973 (1984)
26. T.A. Jackson, E. Yikilmaz, A.F. Miller, T.C. Brunhold, J. Am. Chem. Soc. **125**, 8348–8363 (2003)
27. A.F. Miller, D.L. Sorkin, K. Padmakumar, Biochemistry **44**, 5969–5981 (2005)
28. L.E. Grove, J.K. Hallman, J.P. Emerson, J.A. Halfen, T.C. Brunhold, Inorg. Chem. **47**, 5762–5774 (2008)
29. T.A. Jackson, T.C. Brunold, Acc. Chem. Res. **37**, 461–470 (2004)
30. S. Aime, B. Bergamasco, D. Biglino, G. Digilio, M. Fasano, E. Giamello, L. Lopiano, Biochim. Biophys. Acta **1361**, 49–58 (1997)
31. L. Lopiano, M. Chiesa, G. Digilio, S. Giraudo, B. Bergamasco, E. Torre, M. Fasano, Biochim. Biophys. Acta **1500**, 306–312 (2000)
32. N. Roy, S. Sproules, E. Bill, T. Weyhermuller, K. Wieghardt, Inorg. Chem. **47**, 10911–10920 (2008)